Uncertainty-Informed Operation Coordination in a Water-Energy Nexus

Mohannad Alhazmi, *Member, IEEE*, Payman Dehghanian, *Senior Member, IEEE*, Mostafa Nazemi, *Member, IEEE*, and Konstantinos Oikonomou, *Member, IEEE*

***Abstract*—The widespread deployment of smart heterogeneous technologies and the growing complexity in our modern society calls for effective coordination of the interdependent lifeline networks. In particular, operation coordination of electric power and water infrastructures is urgently needed as the water system is one of the most energy-intensive networks, an interruption in which may quickly evolve into a dramatic societal concern. This paper develops a novel analytic for uncertainty-aware day-ahead operation optimization of the interconnected power and water systems (PaWS). Joint probabilistic constraint (JPC) programming is employed to capture the uncertainties in wind resources and water demand forecasts. The proposed integrated stochastic model is presented as a non-linear non-convex optimization problem, where the non-linear hydraulic constraints in the water network are linearized using piece-wise linearization technique, and the non-convexity is efficiently tackled with a solution methodology to convert the proposed model with JPCs to a tractable mixed-integer linear programming (MILP) formulation that can be quickly solved to optimality. The suggested framework is applied to a 15-node commercial-scale water network jointly operated with a power transmission system using a modified IEEE 57-bus test system. The numerical results demonstrate the of the proposed stochastic framework, resulting in cost reduction (13% on average when compared to the traditional setting) and energy saving of the integrated model under different realizations of uncertain renewable energy sources (RESs) and water demand scenarios. Additionally, the scalability of the proposed model is tested on a modified IEEE 118-bus test system connected to five water networks.**

***Index Terms*—Interdependent networks, joint probabilistic constraints (JPCs), power and water systems (PaWS), water distribution system, water-energy nexus (WEN).**

Manuscript received 19 April 2022; accepted 14 July 2022. Date of publication 2 August 2022; date of current version 4 May 2023. This work was supported by the U.S. National Science Foundation (NSF) under Grant CNS-1951847. Paper no. TII-22-1662. *(Corresponding author: Mohannad Alhazmi.)*

Mohannad Alhazmi is with the Department of Electrical Engineering, College of Applied Engineering, King Saud University, Riyadh 11421, Saudi Arabia (e-mail: alhazmi@gwu.edu).

Payman Dehghanian is with the Department of Electrical and Computer Engineering, George Washington University, Washington, DC 20052 USA (e-mail: payman@gwu.edu).

Mostafa Nazemi is with the MPR Associates, Inc., Alexandria, VA 22314 USA (e-mail: mostafa_nazemi@gwu.edu).

Konstantinos Oikonomou is with the Pacific Northwest National Laboratory (PNNL), Richland, WA 99352 USA (e-mail: konstantinos.oikonomou@pnnl.gov).

Color versions of one or more figures in this article are available at https://doi.org/10.1109/TII.2022.3195695.

Digital Object Identifier 10.1109/TII.2022.3195695

NOMENCLATURE

Sets	
$b \in B$	Set of electric system buses.
$g \in NG$	Set of power generating units.
$k \in L$	Set of power transmission lines.
$w \in W$	Set of wind turbines.
Parameters	
$\mathcal{M}$	Arc-Node $\mathcal{A} \times \mathcal{N}$ incidence matrix.
$\mathcal{C}$	Reservoir-Node $\mathcal{R} \times \mathcal{N}$ incidence matrix.
$\mathcal{K}$	Pump-Arc $\mathcal{P} \times \mathcal{A}$ incidence matrix.
$\mathcal{G}$	Tank-Node $\mathcal{T} \times \mathcal{N}$ incidence matrix.
Θ	Bus-Pump $B \times \mathcal{P}$ incidence matrix.
$P_{w,t}$	Expected wind power forecast of wind farm w at time t (MW).
$P_{b,t}$	Electricity demand at bus b at time t (MW).
$P_{db}^{\max}, P_{db}^{min}$	Maximum/minimum PaWS electricity demand at bus b at time t (MW).
$P_k^{\max}$	Maximum flow limit of transmission line k.
$P_g^{\max}, P_g^{min}$	Maximum/minimum capacity limit of generating unit g (MW).
d_t	Vector of water demand (m^3/sec) at time t.
$\hat{h}$	Reservoirs' geographical height (m).
$q_{(.)}^{\hat{\epsilon}}, q_{(.)}^{\hat{p}}$	Linearized flow rate for pipe ϵ and pump p.
$V^{\max}, V^{min}$	Maximum/minimum volume of water tanks.
$\Delta E^{\max/\min}$	Maximum/minimum of the difference in the water flow rate to water tanks.
$h^{\max}, h^{\min}$	Maximum/minimum nodal pressure heads.
$P^{\mathrm{p,max/min}}$	Maximum/minimum power consumption of water pump p at each bus b (MW).
$c_{0,t}$	Fixed cost coefficients of generating unit g at time t ($).
$c_{g,t}$	linear cost coefficients of generating unit g at time t ($/MW).
$c_{s,t}$	Vector of reservoirs' water price at time t.
$c_{p,t}$	Electricity price of pump p at time t ($/MW).
$q^{\max/\min}$	Maximum/minimum water flow rate though the water network.
$\mathcal{M}$	Water network arc-node incidence matrix.
Variables and Functions	
R_t^s	Vector of water inflow rate from reservoir s at time t.
q_t	Water flow rate at time t.
h_t	Pressure heads loss for node n at time t.
$Sign(.)$	Sign function.

ΔE_t The difference in water tanks' inflow/outflow rate at time t.
T_t^{in} Vector of water inflow to tanks at time t.
T_t^{out} Vector of water outflow to tanks at time t.
V_t Volume of stored water in tanks at time t.
W_t Pumps' speed at time t.
P_t^p Power consumption for pump p at time t.
$P^{p,wd}$ Vector of water electricity consumption wd for pump p at time t.
$X_{i,t}^{\epsilon}$ Continuous decision variable for the sampling coordinate i associated with the linearization of pipe ϵ at time t.
$X_{u,m,t}^{p}$ Continuous decision variable for the sampling coordinates u and m associated with the linearization of pump p at time t.
p_t^w Scheduled wind power at time t.
D_t^l Scheduled water demand at time t (m^3/sec).
$P_{g,t}$ Output power of generating unit g at time t.
$P_{k,t}$ Power flow on transmission line k at time t.
$P_{db,t}$ Total PaWS electricity demand at bus b at time t (MW).
$\theta_{.,t}$ Voltage angle difference between bus n and m at time t.
$\mathcal{K}q_t$ Water flow rate through pump at time t.
$a_{(.)}$, $z_{(.)}$ Pump performance parameters.

Random Variables

$p_t^{w,\text{f}}$ Wind power forecast at time t.
$D_t^{l,\text{f}}$ Water demand forecast at time t (m^3/sec).

Binary Variables

$Y_{i,t}^{\epsilon}$ Binary variable for pressure head breakpoint i of water pipe ϵ at time t.
$h_{u,m,t}^{\text{Upper},p}$ Binary variable for the upper left triangle associated with the linearization of pump p at time t.
$h_{u,m,t}^{\text{Lower},p}$ Binary variable for the lower left triangle associated with the linearization of pump p at time t.

I. Introduction

POWER and water networks (PaWS) are among the critical lifeline infrastructures due to their pivotal roles in backboning our modern society and human life. Water pumps receive a remarkable portion of the total electricity needed to run the water system infrastructure: Around 4% of the total electricity usage in the USA is exhausted by electric pumps in water networks [1]. As the water networks undergo rapid electrification due to the sharp increase in the national population, it calls for improvements in PaWS energy and cost efficiency. Traditionally, PaWS have been independently planned as decoupled systems, while the two networks are operated interdependently in real-world applications [2]. Power systems are in need of water for refining fuels and generating electricity; on the other hand, electricity is needed for the daily operation of water systems. The interdependency in PaWS is further highlighted in the case of limited availability of resources in either system. For instance, if a shortage in cooling water for conventional steam power plants is realized, the water system may not be supplied with the needed energy to pump the water through the network; this could, in turn, result in a cascading failure in both systems. Such lack of coordination was experienced during the hurricane Maria in Puerto Rico [3], where the storm damaged around 90% of the state's electrical system, and large areas were not supplied with water for a long time due to the severance of the hurricane and the lack of coordination between different interconnected sectors, i.e., power and water operators, which resulted in a longer recovery time [4], [5]. This closely-intertwined ecosystem of water and power infrastructures is commonly known as water-energy nexus (WEN) [6].

A literature review on the role of WEN in the optimization of water distribution system is presented in [7]. WEN is analyzed in [8] to investigate the effect of PaWS interdependence on different economic sectors. An approach for the optimal dispatch of PaWS is presented in [9], considering the impacts of battery storage facilities. The authors in reference [10] studies the impacts of power and water economic dispatch on the supply side of the WEN (e.g., hydroelectric and thermal desalination plants). A mathematical codispatch model for the optimal network flows in PaWS is developed in [11]. The authors in reference [12] presented a robust optimization formulation for daily hydro-thermal operation scheduling taking only the water network constraints into account. Energy flexibility through coordination of PaWS is introduced in [13]. The authors in references [14]–[16] introduced a methodology to assess the infrastructural and operational resilience of PaWS under critical conditions (e.g., limited water and/or energy availability). Another scope of research in this area focuses on the optimal demand response and regulation markets for water distribution systems [17], [18].

The aforementioned studies did not effectively capture the critical role of renewable energy sources (RESs), e.g., wind power, in the operation of interconnected PaWS, taking into account the complete model for both power and water systems. Nevertheless, PaWS is facing growing challenges due to the uncertainty in both networks. PaWS operators experience a high level of uncertain RESs, and an increased level of customer demand. Few studies have been conducted to optimize the utilization of RESs in PaWS. A framework for utilizing water pumps and tanks to receive the needed energy for their operation from RESs is proposed in [19]. A cooptimization model for PaWS considering the availability of solar energy is suggested in [20] and [21]. Neither the RESs stochasticity nor the uncertainty in water demand forecast has been well addressed in the literature.

A scenario approach is used in [22] to model the variability of water demand forecasts, while the complete set of water network hydraulic constraints and the RES uncertainty were neglected. Multiobjective optimization for PaWS operation under the uncertainty in river inflows is introduced in [23]. A dynamic multiobjective framework for the operation of WEN in off-grid islands is presented in [24]. The authors in reference [25] models a multiobjective framework for planning WEN

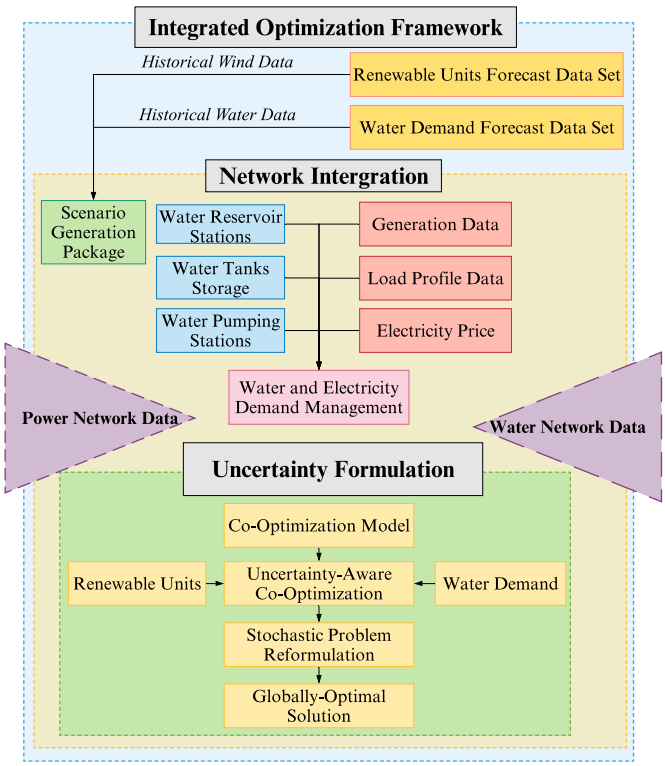

Fig. 1. Overview of the proposed methodology for integrated PaWS.

at regional scales. The robust operation of WEN against the variability of wind generation units is studied in [26]. The uncertainty in PaWS demand at the distribution level is studied in [27]. A two-stage distributionally robust optimization approach is pursued in [28] to model the uncertainty of wind energy sources in WEN, including power, gas, and water systems. However, a complete integration of the PaWS that effectively captures the prevailing stochasticities in both networks need to be further researched.

Different from the conventional practice where the PaWS operation is approached either independently or coordinated through an iterative exchange of status information between both networks, this article bridges the gap in the literature to optimize the operation of interlinked water and power systems under uncertainty. We propose a novel approach for capturing the uncertainties in both networks (i.e., in RESs and water demand) using a joint probabilistic constrained (JPC) formulation. In particular, the proposed model with JPCs enables the operation of PaWS where the entire set of uncertain constraints are enforced to be satisfied with a predefined reliability level. The suggested stochastic formulation with JPCs appears in form of a nonlinear nonconvex optimization model. The proposed formulation is then linearized, convexified, and reformulated through a boolean programming approach into an equivalent mixed-integer linear programming (MILP) formulation to cope with the computational complexity. The proposed reformulation allows for a very fast solution of the stochastic optimization model in which the random variables are represented by a large number of scenarios. Fig. 1 illustrates a big picture of the proposed stochastic framework for integrated operation of the interdependent PaWS under uncertainty. Wind and water demand forecast datasets are collected using historical data for scenario generation. The PaWS operator then uses these data as the input for the PaWS cooptimization engine. The stochasticity of wind power and water demand realizations are captured through the proposed optimization model with JPCs which is then reformulated to a MILP model that ensures the solutions are globally optimal.

The main contributions of this article are as follows.

1) The article proposes an uncertainty-aware mechanism for the operation optimization of the RES-integrated PaWS. Effectively capturing the prevailing uncertainties in RESs and water demand, we introduce new models with JPCs that enforce the entire set of uncertain constraints to be satisfied with a predefined reliability level. The suggested model provides a set of globally optimal solutions with less conservativeness and more flexibility compared to the classical models with individual probabilistic constraint (IPC).
2) A boolean approach is applied to reformulate the proposed stochastic models with JPCs into an equivalent MILP formulation. The employed boolean reformulation requires fewer newly-introduced integer variables, which enhances the computational efficiency of the suggested framework.

The rest of this article is organized as follows. Section II introduces a deterministic model of the coordination framework for PaWS operation utilizing wind units. The proposed formulation with JPCs and the suggested reformulation technique are presented in Section III. Numerical case studies and simulation results on a modified IEEE 57-bus test system integrated with a 15-node water network are demonstrated in Section IV. Finally, Section V concludes this article.

II. Deterministic Problem Formulation

In this section, a deterministic formulation for the integrated operation optimization of PaWS is presented. The components of the water network (e.g., reservoirs, pipes, pumps, and tanks) are mathematically modeled based on a directed graph $G = (\mathcal{N}, \mathcal{A})$, i.e., a set of nodes connected together by pipes directed from one node to another; where $\mathcal{N}$ represents the set of nodes with water sources $s \in \mathcal{S}$ (i.e., reservoirs or tanks) and demand junctions $l \in \mathcal{L}$, i.e., $\mathcal{N} = \{\mathcal{S} \cup \mathcal{L}\}$. Pipelines $\epsilon \in \varepsilon$ and pumps $p \in \mathcal{P}$ are reflected by set $A \in \mathcal{A}$, i.e., $\mathcal{A} = \{\mathcal{P} \cup \varepsilon\}$. Positive and negative values for the water flow rate q defines the direction of each arc [29].

1) Objective Function: The objective function of the proposed optimization model is presented as follows:

$$\min \sum_{t=1}^{NT} \sum_{g=1}^{NG} \sum_{s=1}^{\mathcal{S}} \sum_{p=1}^{\mathcal{P}} \left(c_{0,t} + c_{g,t} P_{g,t} + c_{s,t} R_t^s + c_{p,t} P_t^p \right). \tag{1}$$

The objective function aims to minimize the total operation cost of PaWS over the entire time period NT, and on a system with NG number of generating units, $\mathcal{S}$ number of reservoirs, and

$\mathcal{P}$ number of water pumps. The first two terms in the objective function are the fixed and linear costs of the power generating units. The third term represents the cost incurred by purchasing water from reservoirs. The last term reflects the cost of electricity needed to operate the water pumps. The objective function of the integrated PaWS model is subject to the following set of system and operation constraints.

2) Water Flow Operational Constraints: Water demand is delivered to end users from the reservoirs and tanks through a network of pipes and pumps. The day-ahead water flow constraints are modeled as follows:

$$R_t^s - d_t - \mathcal{M}^{-1} q_t - \mathcal{G}\Delta E_t = 0 \qquad \forall t \qquad (2)$$

$$\Delta E_t = T_t^{in} - T_t^{\text{out}} \qquad \forall t \qquad (3)$$

$$-q^{\max} \le q_t \le q^{\max} \qquad \forall t \qquad (4)$$

$$0 \le \mathcal{K} q_t \le q^{\max} \qquad \forall t \qquad (5)$$

$$R_t^s \ge 0 \qquad \forall t \qquad (6)$$

$$-\mathcal{M} h_t = r_p \mid q_t \mid^{1.852} Sign(q_t) \qquad \forall t \qquad (7)$$

$$\mathcal{C} h_t - \hat{h} = 0 \qquad \forall t \qquad (8)$$

$$h^{\min} \le h_t \le h^{\max} \qquad \forall t \qquad (9)$$

$$V_{t+1} = V_t + \Delta E_t \qquad \forall t \qquad (10)$$

$$V_t = S_a \mathcal{G} h_t \qquad \forall t \qquad (11)$$

$$V^{\min} \le V_t \le V^{\max} \qquad \forall t \qquad (12)$$

$$\Delta E^{\min} \le \Delta E_t \le \Delta E^{\max} \qquad \forall t \qquad (13)$$

$$P^{p,\min} \le P_t^p \le P^{p,\max} \qquad \forall t \qquad (14)$$

$$\mathcal{K}\mathcal{M} h_t = W_t^2 \left(a_1 - a_2 \left(\frac{\mathcal{K} q_t}{W_t} \right)^{a_3} \right) \qquad \forall t \qquad (15)$$

$$P_t^p = W_t^3 \left(z_1 - z_2 \left(\frac{\mathcal{K} q_t}{W_t} \right) \right) \qquad \forall t. \qquad (16)$$

Water flow balance equation is modeled in (2). The difference between the input and output water flow of the tanks, ΔE_t, is modeled in (3). The water flow through pipes is limited in (4), where the positive/negative value of q_t indicates the direction of the water flow rate. Water flow through pumps is bounded in constraint (5). Constraint (6) ensures that only positive values can be taken for water inflow rates at reservoir nodes.

The nodal pressure head loss constraint for water pipes is modeled in (7)–(9). The pressure head loss in water pipes is modeled in (7) by the Hazen–Williams formula [30], where the coefficient r_p depends only on the water flow. Note, the Hazen–Williams formula is a quantitative term used to describe the pressure loss that occurs in water pipes due to friction. The pressure head of the water reservoirs is fixed by its geographical heights in (8). Constraint (9) bounds the nodal pressure at each node in the water network to its maximum and minimum values.

The most challenging components to model within a water network are the tanks and pumps. Water tanks' dynamic operation constraints are modeled in (10)–(14). The water flow balance equation for water tanks is governed by constraint (10). The pressure head at the tank nodes, which is driven by the water stored in the related tanks, is modeled in (11), where S_a is the tank's diagonal surface parameter. Constraint (12) bounds the volume of each tank to its minimum and maximum capacities. The difference between the charging and discharging water flow in tanks is formulated in (13). Pump electricity consumption is limited to its minimum and maximum capacities in (14). The controlled increase in water pump pressure is modeled in constraint (15). The electricity consumption for water pumps is formulated in (16). Note, $a_{(.)}$ and $z_{(.)}$ in constraints (14) and (15) are the pump performance parameters.

3) Linearization Technique: Constraints (1)–(16) represent the complete hydraulic constraints for water networks, and appear in the form of nonlinear programming (NLP) constraints. The nonlinear constraints are presented in (7), (15), and (16). Solving an NLP model can be time-intensive and complex in a large scale water network, which may not result in a feasible solution. In order to guarantee a feasible set of solutions for the optimization problem, a piece-wise linearization technique [29], [31] is applied to the presented nonlinear constraints. In so doing, water flow rate through pipes q_t^ϵ and pumps q_t^p are divided into several breakpoints, i.e., $(\hat{q_1^\epsilon}, \hat{q_2^\epsilon}, \ldots, \hat{q_I^\epsilon})$ and $(\hat{q_1^p}, \hat{q_2^p}, \ldots, \hat{q_U^p})$. In other words, q_t^ϵ axis is divided over the range of the function to segments using $i = 1, 2, 3, \ldots, I$ sampling coordinates (breakpoints) $\hat{q_1^\epsilon}, \hat{q_2^\epsilon}, \ldots, \hat{q_I^\epsilon}$. The breakpoints $(\hat{q_1^\epsilon}, \hat{q_I^\epsilon})$ and $(\hat{q_1^p}, \hat{q_U^p})$ are set at the extremes (i.e., at the maximum and minimum values for q_t^ϵ and q_t^p). Similarly, pump speed W_t is divided into several breakpoints, i.e., $(\hat{w_1}, \hat{w_2}, \ldots, \hat{w_M})$, where $(\hat{w_1}, \hat{w_M})$ coincide with the minimum and maximum values of W_t. A continuous variable for each breakpoint $X_{i,t}^\epsilon \in [0, 1]$ is introduced to approximate the univariate function in (7). Let $Y_{i,t}^\epsilon$ be a binary variable for each pipe ϵ corresponding to the ith interval (i.e., $\hat{q_i^\epsilon}, \hat{q_{i+1}^\epsilon}$). Similarly, bivariate functions for pump p in (15) and (16) are approximated using the triangle technique of the piece-wise linearization. Continuous variable $X_{u,m,t}^p \in [0, 1]$ for each (u, m) is introduced. The binary variables are accordingly associated with the upper triangle $h_{u,m,t}^{\text{Upper},p} (u = 1, .., U; m = 2, .., M)$ and the lower triangle $h_{u,m,t}^{\text{Lower},p} (u = 2, .., U; m = 1, .., M-1)$. The nonlinear constraints (7), (15), and (16) are substituted by the following linear constraints:

$$\sum_{i=1}^{I-1} Y_{i,t}^\epsilon = 1 \qquad \forall \epsilon, \forall t \qquad (17)$$

$$X_{i,t}^\epsilon \le Y_{i-1,t}^\epsilon + Y_{i,t}^\epsilon \qquad \forall i = 2, \ldots, I-1, \forall \epsilon, \forall t \qquad (18)$$

$$\sum_{i=1}^{I} X_{i,t}^\epsilon = 1 \qquad \forall \epsilon, \forall t \qquad (19)$$

$$X_{I,t}^\epsilon \le Y_{I-1,t}^\epsilon \qquad \forall \epsilon, \forall t \qquad (20)$$

$$X_{1,t}^\epsilon \le Y_{1,t}^\epsilon \qquad \forall \epsilon, \forall t \qquad (21)$$

$$q_t^{\epsilon} = \sum_{i=1}^{I} X_{i,t}^{\epsilon} \hat{q_i^{\epsilon}} \qquad \forall \epsilon, \forall t \qquad (22)$$

$$\Delta h_t^{\epsilon} = \sum_{i=1}^{I} X_{i,t}^{\epsilon} \Delta h_t^{\epsilon}(\hat{q_i^{\epsilon}}) \qquad \forall \epsilon, \forall t \qquad (23)$$

$$\sum_{u=1}^{U} \sum_{m=1}^{M} X_{u,m,t}^{p} = 1 \qquad \forall p, \forall t \qquad (24)$$

$$\sum_{u=1}^{U} \sum_{m=1}^{M} (h_{u,m,t}^{\text{Upper},p} + h_{u,m,t}^{\text{Lower},p}) = 1 \qquad \forall p, \forall t \qquad (25)$$

$$X_{u,m,t}^{p} \le h_{u,m-1,t}^{\text{Upper},p} + h_{u+1,m,t}^{\text{Upper},p} + h_{u,m,t}^{\text{Upper},p} + h_{u-1,m,t}^{\text{Lower},p} + h_{u,m+1,t}^{\text{Lower},p} + h_{u,m,t}^{\text{Lower},p} \quad \forall u, \forall m, \forall p, \forall t \qquad (26)$$

$$q_t^{p} = \sum_{u=1}^{U} \sum_{m=1}^{M} X_{u,m,t}^{p} \hat{q_u^{p}} \qquad \forall p, \forall t \qquad (27)$$

$$W_t = \sum_{u=1}^{U} \sum_{m=1}^{M} X_{u,m,t}^{p} \hat{w_m^{p}} \qquad \forall p, \forall t \qquad (28)$$

$$\Delta h_t^{p} = \sum_{u=1}^{U} \sum_{m=1}^{M} \Delta h_t^{p}(\hat{q_u^{p}}, \hat{w_m^{p}}) X_{u,m,t}^{p} \qquad \forall p, \forall t \qquad (29)$$

$$P_t^{p} = \sum_{u=1}^{U} \sum_{m=1}^{M} P_t^{p}(\hat{q_u^{p}}, \hat{w_m^{p}}) X_{u,m,t}^{p} \qquad \forall p, \forall t. \qquad (30)$$

The pressure head difference in water pipes h_t^{ϵ} (i.e., $\Delta h_t^{\epsilon} = h_{n,t}^{\epsilon} - h_{n+1,t}^{\epsilon}$) in (7) is approximated by constraints (17)–(23). Constraint (17) enforces only one binary variable $Y_{i,t}^{\epsilon}$ to take a nonzero value. Constraints (18)–(21) imply that only values other than zero are chosen for a pair of consecutive positive continuous variables $X_{i,t}^{\epsilon}$ and $X_{i+1,t}^{\epsilon}$. Constraint (22) can uniquely represent any given point for the water flow rate through pipes q_t^{ϵ}, as it is the linear combination of two successive breakpoints weighted by the associated variables $X_{i,t}^{\epsilon}$. Constraint (23) ensures that the pressure difference for each pipe Δh_t^{ϵ} is properly chosen for the accurate computation of the approximated values.

Water flow through pumps, pressure head difference, and the electricity consumption by water pumps in (15) and (16) are approximated by constraints (24)–(30). The weights of the convex combination for the selected triangle is introduced in (24). Constraint (25) ensures that only one triangle is used for the convex combination. Constraint (26) enforces that only nonzero values of $X_{u,m,t}^{p}$ can be associated with the three vertices of the triangle. Constraints (27) and (28) represent the linear combinations of any values for q_t^{p} and W_t, weighted by the continuous variables $X_{u,m,t}^{p}$, respectively. The bivariate nonlinear functions for the increase in pressure difference in each water pump Δh_t^{p} (i.e., $\Delta h_t^{p} = h_{n+1,t}^{p} - h_{n,t}^{p}$) and the power consumption of pumps P_t^{p} are approximated in (29) and (30), respectively.

4) PaWS Integration Constraints: Power system's DC optimal power flow mechanism is integrated with the water network through the following constraints:

$$P_t^{p,wd} = \sum_{p=1}^{\mathcal{P}} \Theta P_t^{p} \qquad \forall t \qquad (31)$$

$$P_{db,t} = P_{b,t} + P_t^{p,wd} \qquad \forall b, \forall t \qquad (32)$$

$$P_{db}^{\min} \le P_{db,t} \le P_{db}^{\max} \qquad \forall b, \forall t \qquad (33)$$

$$P_{k,t} = \frac{\theta_{n,t} - \theta_{m,t}}{x_k} \qquad \forall k, \forall t \qquad (34)$$

$$-P_k^{\max} \le P_{k,t} \le P_k^{\max} \qquad \forall k, \forall t \qquad (35)$$

$$P_g^{\min} \le P_{g,t} \le P_g^{\max} \qquad \forall g, \forall t \qquad (36)$$

$$\sum_{g \in NG} P_{g,t} + \sum_{w \in W} P_{w,t} - \sum_{k \in L} P_{k,t} = \sum_{d \in D_i} P_{db,t} \qquad \forall t. \qquad (37)$$

The incidence matrix Θ is introduced in constraint (31) to map the dimension of P_t^{p} to the power system buses. Constraint (32) sums the total electricity demand for power and water networks together. Electricity consumption at each load point is bounded in (33). Constraint (34) sets the power flow in each transmission line. The power flow in each transmission line is bounded to the minimum and maximum capacity limits in (35), where the positive/negative value of $P_{k,t}$ indicates the direction of the power flow on transmission lines. The output power of the system generating units is limited to the minimum and maximum capacity limits in (36). System power balance constraint is enforced in (37).

The complete deterministic problem formulation (DPF) in the form of an MILP optimization model is presented in the following, which considers the integrated operation of power and water networks utilizing wind resources:

$$\textbf{DPF}: \min\ (1)$$
$$\text{subject to}\ \ (2)-(6), (8)-(14), (17)-(37).$$

III. Proposed Problem Formulation With JPCs

The deterministic MILP model ignores the uncertainties in wind energy as well as water demand forecasts; i.e., it assumes a perfect knowledge of the forecasted wind power and water demand, which results in suboptimal solutions. A JPC problem formulation is suggested that can effectively capture such uncertainties in both networks.

A. JPC Formulation

The proposed problem formulation with JPCs, i.e., joint probabilistic constrained problem formulation (JPC-PF), is presented

in the following:

$$\mathbf{JPC-PF}: \ \min (1)$$
$$\text{subject to} \quad (3)-(6),(8)-(14),(17)-(36)$$
$$R_t^s - D_t^l - \mathcal{M}^{-1} q_t - \mathcal{G}\Delta E_t = 0 \qquad \forall t \quad (38)$$
$$\sum_{g\in NG} P_{g,t} + \sum_{w\in\mathcal{W}} p_t^w - \sum_{k\in L} P_{k,t} = \sum_{d\in D_i} P_{db,t} \qquad \forall b, \forall t \quad (39)$$
$$\mathbb{P}\left(\begin{matrix} p_t^w \le p_t^{w,\mathrm{f}}, \ \forall w, \ \forall t \\ D_t^l \le D_t^{l,\mathrm{f}}, \ \forall l, \ \forall t \end{matrix}\right) \ge \kappa \quad (40)$$

where (38) and (39) represent the water flow balance and nodal power balance constraints, respectively, considering the stochasticity of wind power p_t^w and water demand realizations D_t^l. The JPC (40) enforces wind power and water demand realizations to be always equal to or less than the forecasted values with a predefined reliability level κ. Note that each random variable is associated with a discrete probability distribution at each time interval. The notation κ is set by the PaWS operators based on the preferred and allowable violation level in the system. That is, the higher the desired reliability level is, the more conservative the solution is and thus the lower the number of the violated scenarios will be. Note that the random variables are not present in the objective function, as we do not intend to minimize wind power or water demand.

B. Solution Methodology: A Boolean Approach

In this section, boolean reformulation method is suggested to solve the introduced model with JPCs. The boolean reformulation method [32]–[34] effectively tackles the computational challenges of solving the stochastic problem with JPCs. The boolean approach constructs a set of *recombinations*, *binarization*, and *reformulation*. The boolean framework is succinctly described in Fig. 2, which can operate in three successive stages: 1) initialization; 2) κ-sufficiency; 3) binarization process. In the initialization stage, all possible realizations of the random variables are defined and the cumulative distribution function of each realization is obtained. Next, in the κ-sufficiency process, the sufficient/insufficient cut points associated with κ are obtained. Eventually, in the binarization process, the binary variable vectors of β are defined based on the realization of random variables and the value of cut points obtained in the previous step. The newly introduced binary variables will then be used in the reformulation equations.

Note that F denotes the cumulative distribution function of the random variable ξ. The set Ω, describing the set of all possible realizations ω^k of the random variable ξ with dimension J, is divided into two decoupled sets of κ-sufficient, i.e., Ω^+, and κ-insufficient, i.e., Ω^-, such that any recombination k belongs to either Ω^+ or Ω^-. It should be noted that $\Omega^+ \cap \Omega^- = \emptyset$. The notation β_{ij} reflects the ith binary associated with each element ξ_j. c_{ij} denotes the ith component of ξ_j. Moreover, $g(k)$ gets the value 1 if the realization k belongs to κ-sufficient, i.e., Ω^+, and gets 0, otherwise. Notation C^e reflects the sufficient

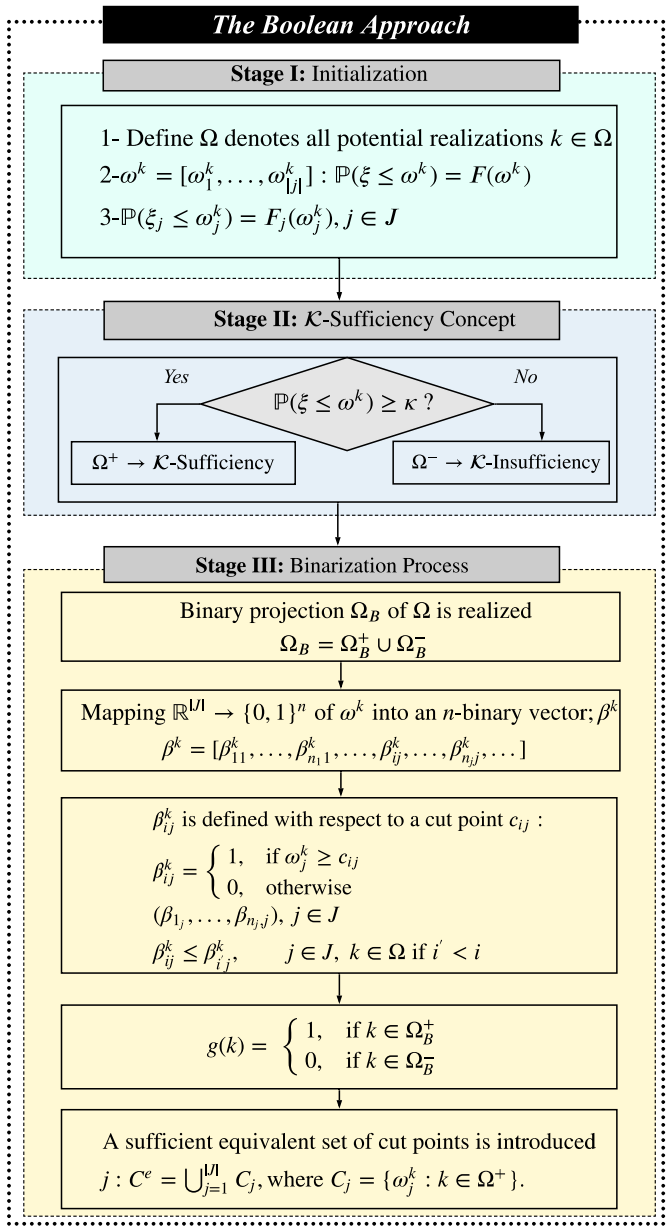

Fig. 2. Overall implementation procedure of the boolean algorithm.

equivalent set of cut points where it accepts any k-sufficient realization on any component j. In summary, the probability distributions represent the feasibility of the JPCs with partially defined boolean functions (pdBf) and the binary images of the recombinations allow for modeling the feasible area of (40) with a pdBf from which, a system of mixed-integer inequalities can be extracted to represent exactly the feasible region of the JPCs. All random variables considered here have a discrete distribution function, which is one of the advantages of using the boolean reformulation approach. In other words, the applied boolean approach does not require a continuous probability distribution function for the forecasted random variables. Instead, the random variables can be represented with a discrete distribution function. Any random values can be defined in a specified range of forecasts for both water demand and wind generation. The

proposed JPC-PF is here reformulated to an equivalent MILP model. The solution of the proposed reformulation concurrently allows for: 1) the generation of minimal conditions for the JPCs (40) to hold; 2) the reformulation and exact solution of the formulated stochastic problem. The proposed MILP reformulation of the original problem JPC-PF is illustrated as follows:

$$\mathbf{REF-JPC}: \min (1)$$

$$\text{s.t.} \quad (3)-(6),(8)-(14),(17)-(36),(38)-(39)$$

$$p_t^w \geq \sum_{j=1}^{n_t} c_{jt} u_{jt} \qquad \forall w, \forall t \quad (41)$$

$$D_t^l \geq \sum_{j=1}^{n_t} c'_{jt} u'_{jt} \qquad \forall l, \forall t \quad (42)$$

$$\sum_{t\in T}\sum_{j=1}^{n_t} \beta_{jt}^{k} u_{jt} \leq |T|-1 \qquad \forall k \in \bar{\Omega_B^-} \quad (43)$$

$$\sum_{t\in T}\sum_{j=1}^{n_t} \beta_{jt}'^{k'} u'_{jt} \leq |T|-1 \qquad \forall k' \in \bar{\Omega_B'^-} \quad (44)$$

$$\sum_{j=1}^{n_t} u_{jt} = 1 \qquad \forall t \quad (45)$$

$$\sum_{j=1}^{n_t} u'_{jt} = 1 \qquad \forall t \quad (46)$$

$$u_{jt}, u'_{jt} \in \{0,1\} \qquad \forall j = 1,\ldots,n_t, \forall t. \quad (47)$$

Constraints (41)–(47) represent the mixed-integer linear equivalent reformulation of constraint (40) where the uncertainty of wind generation units and water demand are taken into account using JPCs formulation. Constraints (41) and (42) represent the realization of wind generation units p_t^w and water demand D_t^l at each time period t based on the cut points found in the reformulation process, i.e., c_{jt} and c'_{jt}, as well as newly introduced binary variables, i.e.,u_{jt} and u'_{jt} used in the reformulation. The binarization equations are represented in constraints (43) and (44). Constraints (45), (46), and (47) ensure only one binary variable associated with wind generation units u_{jt} and water demand u'_{jt} get a nonzero value. The notation $|T|$ refers to the cardinality of the set T, p_t^w and D_t^l are $|T|$-dimensional random vectors ξ and ξ'; Ω and Ω' are, respectively, the sets of possible realizations $k \in \Omega$ and $k' \in \Omega'$ of the $|T|$-dimensional random vector ξ and ξ' with cumulative distribution function F and F', respectively. The notation β_{jt} and β'_{jt} refer to the jth binary attribute associated with component ξ_t and ξ'_t, respectively. Also, c_{jt} and c'_{jt} denote the jth cut point associated with component ξ_t and ξ'_t, respectively. Note that u_{jt} and u'_{jt} are decision variables corresponding to β_{jt} and β'_{jt}, recpectively.

IV. Numerical Results

A. System Descriptions, Data, and Assumptions

The proposed formulation for the integrated operation optimization of PaWS considering the uncertainties in wind and water demand forecasts is implemented on a modified IEEE 57-bus test system connected to a water network. The water network consists of 15 nodes and is connected to a load point in power grid [13]. The water system includes one reservoir, 11 pipelines, three pumps, and two tanks. Water demand junctions are located at nodes 3, 11, and 15 of the water network. Tanks are set to be empty at the initial time. To further demonstrate the efficiency and scalability of the proposed model, the proposed framework is applied to a larger-scale network with additional number of water networks, i.e., five water networks, each consisting of 15 nodes supplied by the IEEE 118-bus power test system. All data for the studied PaWS and the schematic diagram of both systems are provided in an electronic appendix available in [35]. All simulations are performed in a mathematical programming language (AMPL) environment [36] and MATLAB, using a PC with an Intel Xeon E5-2620 v2 processor, 16 GB of memory, and a 64-b operating system. CPLEX solver is used to simulate and solve the reformulated MILP model.

B. IEEE 57-Bus Test System Connected to a Water Network

1) Case Studies and Results: In order to illustrate the performance of the proposed optimization model, the following four different cases are studied.

1) Case I represents the traditional setting for the operation of PaWS (benchmark scenario), where PaWS are operated independently. In this case, the water system operator's goal is to minimize the purchase cost of water in the network.
2) Case II illustrates the performance of the proposed integrated PaWS operation under the variability of water demand only.
3) Case III represents the optimization model of PaWS considering the uncertainty in wind generation units only.
4) Case IV demonstrates the cooptimized operation of PaWS capturing the prevailing uncertainties in both networks, i.e., wind power and water demand forecasts, modeled with the proposed formulation with JPCs and solved with the boolean technique suggested in Section III. A wind farm with a total installed capacity of 250 MW is located at node 38 of the power network.

A summary of the scheduled day-ahead optimization results in all cases are tabulated in Table I. In Case I, the total operation cost is reported to be \$55 165.8 with a total of 31 506.9 m^3/h water purchased from the reservoir. The total electricity required to pump the water through the network is found to be 173.37 MW. The operation cost of the proposed integrated model for PaWS is reduced in Case II to \$47 497.1 with a total of 109.30 MW energy consumed by water network and 30 920.62 m^3/h of purchased water over 24 h. The operational cost for Case III, where only wind uncertainty is taken into account, is reported at \$47084.71 with a total of 111.89 MW energy consumed by water pumps. The reservoir in Case III supplies the water network with 31 506.51 m^3/h of water. Case IV results in a total operation cost of \$47 608.93 when the proposed uncertainty modeling approach is applied. The amount of water purchased from the reservoir

TABLE I
SUMMARY OF THE OPTIMIZATION RESULTS FOR THE DAY-AHEAD OPERATION SCHEDULES IN PAWS: IEEE 57-BUS TEST SYSTEM

Case #	Operation cost ($)	Pump electricity consumption (MW)	Purchased water (m^3/h)	Number of variables	Number of scenarios		Wind penetration (%)	Computational time (sec)
					Wind	Water demand		
Case I	55 165.88	173.37	31 506.9	15 984	1	1	15.3	100.937
Case II	47 497.1	109.30	30 920.62	16 038	1	24,000	15.3	173.23
Case III	47 084.71	111.89	31 506.51	16 043	24,000	1	13.87	109.60
Case IV	47 608.93	108.33	30 919.87	16 097	24,000	24,000	13.8	208.8

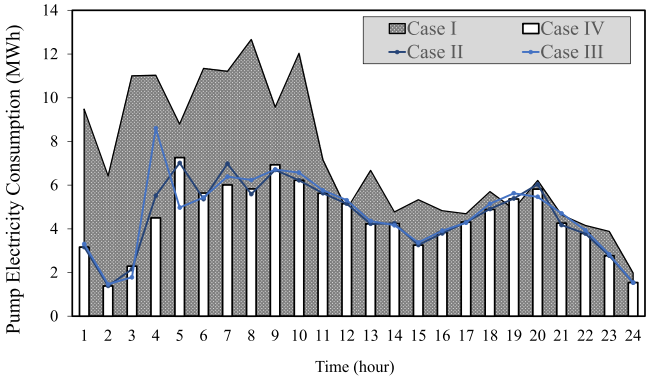

Fig. 3. Pump electricity consumption in different test cases: IEEE 57-bus test system.

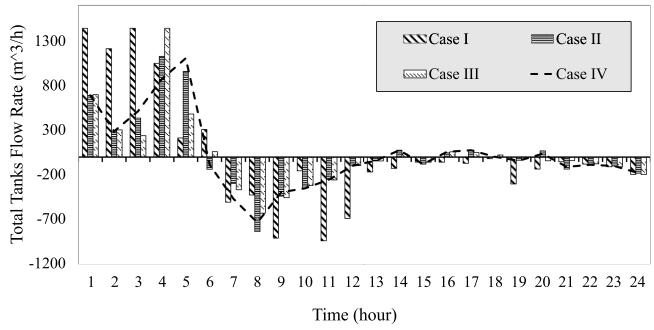

Fig. 4. Total flow rate schedules for water tanks: IEEE 57-bus test system.

in Case IV is found 30 919.87 m^3/h and the total electricity consumed by the water network is obtained in this case equal to 108.33 MW. The operation cost in Case IV, when the proposed stochastic formulation with JPCs is applied, is lower than that in Case I (benchmark scenario). Wind supplies 13.8% of the total electricity demand in Case IV and 13.87% in Case III, compared to 15.3% in Cases I and II. This is because the wind forecast at each time period is assumed with one mean-value scenario in Cases I and II, while a total number of 1000 scenarios are considered for wind forecast at each time period (a total of 24 000 scenarios for 24 time periods) in Cases III and IV. As expected, one can observe that the stochastic approach results in more accurate solutions as it captures different scenarios. Moreover, while the purchased water is observed almost the same in all studied test cases, the pump usage in the water network is more efficient in Case IV compared to the traditional approach in Case I. To further clarify, the scheduled electricity demand for water pumps in all cases is illustrated in Fig. 3; one can notice that during off-peak hours, water pumps in Case I consume higher amount of energy compared to the proposed Cases II-IV. The scheduled flow rates for storage tanks in all cases is presented in Fig. 4, where it can be seen that the utilization of water tanks is optimal in Case IV, when the operation of the water network is cooptimized with that of the power network, taking into account the uncertainties in both systems. In Fig. 4, water tanks are charged during off-peak hours (positive value) and discharge to supply the water demand (negative value) during peak hours in order to save the energy consumption by electric pumps. In summary, the critical components of the water systems, i.e., pumps and tanks, are employed more efficiently when the proposed approach in Case IV is implemented.

2) Computational Efficiency: In the proposed model, the random variables ξ_t and ξ'_t refer to the real wind power and water demand forecasts ($p_t^{w,\mathrm{f}}$, $D_t^{l,\mathrm{f}}$), respectively. Each random variable is associated with one single time period; hence, ξ is a random vector with a 24×1 dimension. A total number of 24 000 scenarios (1,000 per hour) for the wind power forecast and 24 000 scenarios (1,000 per hour) for the water demand forecast during the entire 24-h scheduling horizon are generated and the confidence level, κ, is set at 90%. The κ is set to be 90% as it gives the operators pretty good flexibility in allowing for violating scenarios. The higher the κ, e.g., greater than 90%, results in a more conservative solution and may not be practical. The lower the κ, on the other hand, results in a less accurate result, while the flexibility can be higher. Thus, 90% is a good tradeoff for system operators to accommodate the violated scenarios in the PaWS. Fig. 5(a) and (b), respectively, demonstrate the upper and lower bounds for the forecasted values of the uncertainty sources in PaWS where the scheduled wind power and water demand are marked with a solid line. One can see that the realizations of wind and water obtained by the optimization process are always within the range of the forecasts at each time slot. The computational time needed to solve the reformulated stochastic problem using the CPLEX solver is 208.8 s in Case IV, while it is reported at 173.23 s and 109.60 s in Cases II and III, respectively. One can notice that while the total number of scenarios to capture both wind power and water demand forecast uncertainties in Case IV is 48 000 (i.e., 24 000 each), the total number of new binary variables for problem reformulation is 96 in which 90 combinations are κ-insufficient and 6 combinations are κ-sufficient. Note that the total number of variables in Case IV, when uncertainties in both networks are taken into account, is 16 097 throughout the optimization process. Therefore, the boolean reformulation technique suggested to solve the proposed JPCs permits a very

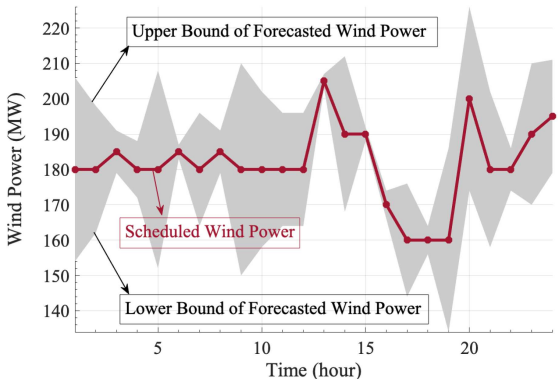

(a)

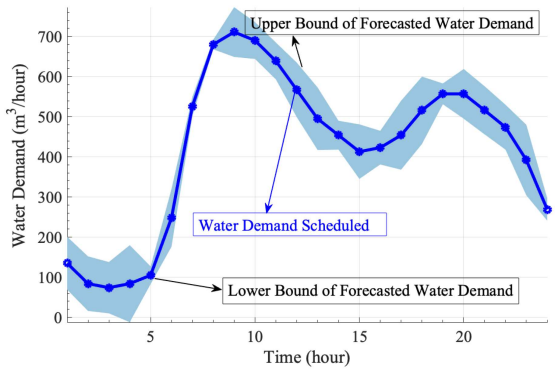

(b)

Fig. 5. Forecasted and scheduled wind power and water demand: IEEE 57-bus test system.

fast solution of the stochastic optimization model in which the random variables are represented by an unprecedentedly large number of scenarios with *discrete distribution functions*.

C. IEEE 118-Bus Test System Supplying Multiple Water Networks

1) Case Studies and Results: The proposed formulation is applied to a larger-scale test system to further study its efficiency and scalability. A modified IEEE 118-bus power test system connected to three water networks is used in this study. Each water network consists of 15 nodes (i.e., a total of 45 nodes) connected to the power system at buses 39, 74, and 102. There are three wind generation units located at buses 8, 33, and 75. The enforced reliability level κ is set at 90%.

The operation cost of the proposed interlinked model of PaWS is reported at \$107 968.58. The total electricity required to pump the water through the three water networks is found to be 344.63 MW, with a total of 92 753.75 m^3/h water purchased from the reservoirs. To further illustrate the performance on a large-scale system, the scheduled electricity demand for water pumps as well as the hourly purchased water from reservoirs in all three water networks are illustrated in Fig. 6. Water tanks' performance in all three water networks are demonstrated in Fig. 7. The computational time required to solve the reformulated model is found at 316.41 s. In summary, the operational results of the proposed PaWS under the presence of stochasticity in both networks reveal that the proposed framework is scalable

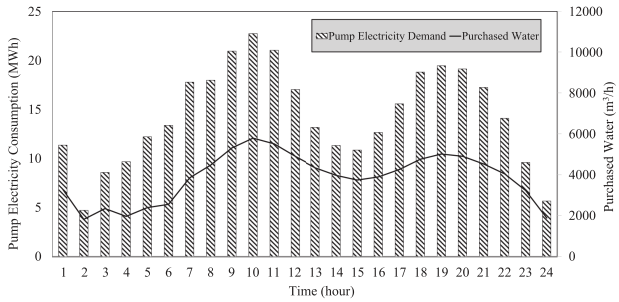

Fig. 6. Total pump electricity consumption and purchased water in all three networks: IEEE 118-bus test system.

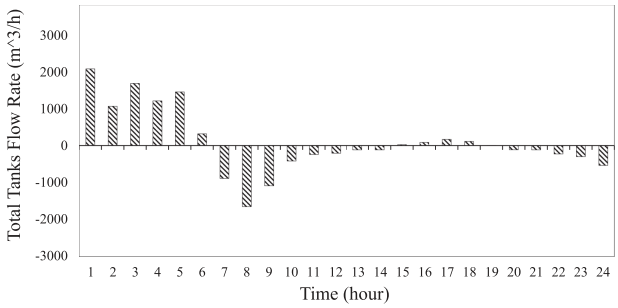

Fig. 7. Total flow rate schedules for water tanks in all three water networks: IEEE 118-bus test system.

TABLE II
PAWS PERFORMANCE ANALYSIS UNDER DIFFERENT CASE STUDIES: IEEE 118-BUS TEST SYSTEM

Case #	Operation cost (\$)	Number of variables	Computational time (sec)
Case I	135 715.76	21 871	432.1
Case II	151 564.1	21 720	413.93
Case III	149 818.7	22 424	489.35
Case IV	151 649.07	26 040	951.1

and computationally efficient when applied to a large-scale PaWS system.

2) Performance Comparison With the State-of-the-Art: In order to demonstrate the performance of the proposed framework compared to other techniques used in the literature, four different cases are investigated in this section using a modified IEEE 118-bus test system connected to five water networks. The water networks are connected to the power system at buses 1, 27, 39, 74, and 102; three wind generation units are located in buses 8, 33, and 75 (see electronic appendix [35]). Case I models the stochasticity of wind units and water demand in PaWS using the proposed model with JPC with a predefined reliability level κ at 90%. Case II studies the stochasticity in PaWS using the proposed model with JPC with a higher reliability level, i.e., κ at 95%. Case III models the stochasticity of wind units and water demand in PaWS using IPCs, which enforce the probability function in (40), defined in the manuscript, to be satisfied individually and at each time period, with a predefined reliability level κ set to 90%. Case IV employs a traditional scenario approach for tackling the variability of wind units and water demand.

Table II demonstrates the performance of the day-ahead operation optimization model for PaWS in different case studies. In

Case I, where κ is set at 90% using the proposed model with JPC, the operational cost is found at \$135 715.76. A total of 21 871 variables are reported in Case I, and the computational time needed to solve the reformulated stochastic problem using the CPLEX solver is 432.1 s. The operational cost in Case II, where the reliability level is set at 95%, has increased to \$151564.1. The total number of variables in Case II is found at 21 720 and the computational time at 413.93 s. When the model with IPC is employed in Case III with a predefined reliability level of 90%, the total operation cost is reported at \$149 818.7. The total number of variables required to solve the model with IPC in Case III is found at 22 424, with a solving time reported at 489.35 s. For the scenario-based approach in Case IV, the total operation cost is found to be \$151649.07. The number of variables used to solve the stochastic model in Case IV is reported at 26 040, and the time required to solve the model is reported at 951.1 s.

It can be observed from Case I and Case II that higher κ results in a more conservative solution and a higher operational cost, as the forecast accuracy for wind generation units and water demand are set at a higher probability, i.e., 95%. Comparing the proposed model with JPC in Case I and the models with IPC in Case III, where the violation level is set at 90% in both cases, one can conclude that the proposed framework results in a less operational cost and lower computational time. Not only is the computational time higher in Case III, but also the number of variables required to solve the problem is higher. The model with IPC applies the violation level 90% at each hour, which results in a 10% violation at each hour, while the proposed JPC enforces the 90% κ for all time periods (i.e., $t = 1..T$) and allows only 10% of scenarios to be violated in all time periods. Comparing the proposed framework in Case I with the scenario-based approach in Case IV, it can be observed that modeling the uncertainty using the scenario approach is time consuming. In summary, employing the proposed methodology to model the uncertainties in PaWS results in less computational complexity and reduces the cost of operating the interconnected networks.

V. Conclusion

Different from the state-of-the-art models, this article proposed a comprehensive day-ahead optimization framework for the coordinated operation under uncertainty of systems in a water-energy nexus under uncertainty. DC optimal power flow constraints were efficiently integrated with the complete water network constraints. The stochasticity in wind power and water demand forecasts was captured through a stochastic formulation with JPCs. A computationally-efficient boolean methodology was used to reformulate and solve the stochastic problem with JPCs. The proposed formulation was applied to a 15-node water network connected to a modified IEEE 57-bus test system. To further demonstrate the efficiency and scalability of the proposed model on large-scale test systems, the proposed framework was applied to a second case study, i.e., various water networks, each consisting of 15 nodes, supplied by the IEEE 118-bus power test system. The simulation results revealed that the proposed framework for cooptimization of interdependent power and water infrastructures results in energy and cost-saving under uncertainty compared to the traditional setting where both networks operate independently. The simulation results showed that the reformulation approach used in this article allows for a computationally efficient solution of the stochastic optimization model.

Future research may include expanding the proposed JPC model to capture uncertainties in electrical loads in power systems. Furthermore, practical implementation requirements of the proposed framework considering hardware components could be further researched. Finally, another scope of research may investigate the operation stability and reliability of the interlinked PaWS.

References

[1] B. Appelbaum, "Water & sustainability (volume 4): US electricity consumption for water supply & treatment—The next half century," Elect. Power Res. Inst., Palo Alto, CA, USA, Rep. 1006787, 2002.

[2] S. Shin et al., "A systematic review of quantitative resilience measures for water infrastructure systems," *Water*, vol. 10, no. 2, 2018, Art. no. 164.

[3] P. Brown et al., "Hurricanes and the environmental justice island: Irma and Maria in Puerto Rico," *Envir. Justice*, vol. 11, no. 4, pp. 148–153, 2018.

[4] R. Subramanian et al., "Air quality in Puerto Rico in the aftermath of hurricane Maria: A case study on the use of lower cost air quality monitors," *ACS Earth Space Chem.*, vol. 2, no. 11, pp. 1179–1186, 2018.

[5] Y. Lin et al., "Impact of hurricane Maria on drinking water quality in Puerto Rico," *Envir. Sci. Technol.*, vol. 54, no. 15, pp. 9495–9509, 2020.

[6] Q. Li, S. Yu, A. Al-Sumaiti, and K. Turitsyn, "Modeling and co-optimization of a micro water-energy nexus for smart communities," in *Proc. IEEE PES Innov. Smart Grid Technol. Conf. Europe*, 2018, pp. 1–5.

[7] N. Vakilifard, M. Anda, P. A. Bahri, and G. Ho, "The role of water-energy nexus in optimising water supply systems-review of techniques and approaches," *Renewable Sustain. Energy Rev.*, vol. 82, pp. 1424–1432, 2018.

[8] D. Fang and B. Chen, "Linkage analysis for the water-energy nexus of city," *Appl. Energy*, vol. 189, pp. 770–779, 2017.

[9] A. Santhosh, A. M. Farid, and K. Youcef-Toumi, "The impact of storage facility capacity and ramping capabilities on the supply side economic dispatch of the energy-water nexus," *Energy*, vol. 66, pp. 363–377, 2014.

[10] A. Santhosh, A. M. Farid, and K. Youcef-Toumi, "Real-time economic dispatch for the supply side of the energy-water nexus," *Appl. Energy*, vol. 122, pp. 42–52, 2014.

[11] A. Santhosh, A. M. Farid, and K. Youcef-Toumi, "Optimal network flow for the supply side of the energy-water nexus," in *Proc. IEEE Int. Workshop Inteligent Energy Syst.*, 2013, pp. 155–160.

[12] H. Zhang, J. Zhou, N. Fang, R. Zhang, and Y. Zhang, "Daily hydrothermal scheduling with economic emission using simulated annealing technique based multi-objective cultural differential evolution approach," *Energy*, vol. 50, pp. 24–37, 2013.

[13] K. Oikonomou and M. Parvania, "Optimal coordination of water distribution energy flexibility with power systems operation," *IEEE Trans. Smart Grid*, vol. 10, no. 1, pp. 1101–1110, Jan. 2019.

[14] S. Zuloaga, P. Khatavkar, L. Mays, and V. Vittal, "Resilience of cyber-enabled electrical energy and water distribution systems considering infrastructural robustness under conditions of limited water and/or energy availability," *IEEE Trans. Eng. Manag.*, vol. 69, no. 3, pp. 639–655, Jun. 2022.

[15] M. Alhazmi, P. Dehghanian, M. Nazemi, F. Wang, and A. Alfadda, "Optimal operation of integrated water-power systems under contingencies," *IEEE Trans. Ind. Appl.*, vol. 58, no. 4, pp. 4350–4358, Jul./Aug. 2022.

[16] M. Alhazmi, P. Dehghanian, M. Nazemi, and F. Wang, "Coordination framework for integrated operation of water-power systems under contingencies," in *Proc. IEEE Ind. Appl. Soc. Annu. Meeting*, 2021, pp. 1–7.

[17] K. Oikonomou, M. Parvania, and R. Khatami, "Optimal demand response scheduling for water distribution systems," *IEEE Trans. Ind. Informat.*, vol. 14, no. 11, pp. 5112–5122, Nov. 2018.

[18] K. Oikonomou and M. Parvania, "Optimal participation of water desalination plants in electricity demand response and regulation markets," *IEEE Syst. J.*, vol. 14, no. 3, pp. 3729–3739, Sep. 2020.

[19] D. Fooladivanda, A. D. Domínguez-García, and P. W. Sauer, "Utilization of water supply networks for harvesting renewable energy," *IEEE Trans. Control Netw. Syst.*, vol. 6, no. 2, pp. 763–774, Jun. 2019.

[20] Q. Li, S. Yu, A. S. Al-Sumaiti, and K. Turitsyn, "Micro water-energy nexus: Optimal demand-side management and quasi-convex hull relaxation," *IEEE Trans. Control Netw. Syst.*, vol. 6, no. 4, pp. 1313–1322, Dec. 2019.
[21] A. S. Zamzam, E. Dall'Anese, C. Zhao, J. A. Taylor, and N. D. Sidiropoulos, "Optimal water-power flow-problem: Formulation and distributed optimal solution," *IEEE Trans. Control Netw. Syst.*, vol. 6, no. 1, pp. 37–47, Mar. 2019.
[22] A. Stuhlmacher and J. L. Mathieu, "Chance-constrained water pumping managing power distribution network constraints," in *Proc. North Amer. Power Symp.*, 2019, pp. 1–6.
[23] J. M. Gonzalez et al., "Spatial and sectoral benefit distribution in water-energy system design," *Appl. Energy*, vol. 269, 2020, Art. no. 114794. [Online]. Available: https://www.sciencedirect.com/science/article/pii/S0306261920303068
[24] F. Giudici, A. Castelletti, E. Garofalo, M. Giuliani, and H. R. Maier, "Dynamic, multi-objective optimal design and operation of water-energy systems for small, off-grid islands," *Appl. Energy*, vol. 250, pp. 605–616, 2019.
[25] S. C. Parkinson, M. Makowski, V. Krey, K. Sedraoui, A. H. Almasoud, and N. Djilali, "A multi-criteria model analysis framework for assessing integrated water-energy system transformation pathways," *Appl. Energy*, vol. 210, pp. 477–486, 2018.
[26] C. Wang, N. Gao, J. Wang, N. Jia, T. Bi, and K. Martin, "Robust operation of a water-energy nexus: A multi-energy perspective," *IEEE Trans. Sustain. Energy*, vol. 11, no. 4, pp. 2698–2712, Oct. 2020.
[27] A. Stuhlmacher and J. L. Mathieu, "Chance-constrained water pumping to manage water and power demand uncertainty in distribution networks," *Proc. IEEE*, vol. 108, no. 9, pp. 1640–1655, Sep. 2020.
[28] P. Zhao et al., "Water-energy nexus: A mean-risk distributionally robust co-optimization of district integrated energy systems," *IEEE Trans. Power Syst.*, vol. 36, no. 3, pp. 2542–2554, May 2021.
[29] M. Alhazmi and P. Dehghanian, "Optimal integration of interconnected water and electricity networks," *IET Gener., Transmiss. Distrib.*, vol. 15, no. 14, pp. 2033–2043, 2021.
[30] L. W. Mays, *Water Resources Engineering*. Hoboken, NJ, USA: John Wiley & Sons, Inc., 2010.
[31] M. Alhazmi, P. Dehghanian, M. Nazemi, and M. Mitolo, "Joint operation optimization of the interdependent water and electricity networks," in *Proc. IEEE Ind. Appl. Soc. Annu. Meeting*, 2020, pp. 1–7.
[32] M. Nazemi, P. Dehghanian, X. Lu, and C. Chen, "Uncertainty-aware deployment of mobile energy storage systems for distribution grid resilience," *IEEE Trans. Smart Grid*, vol. 12, no. 4, pp. 3200–3214, Jul. 2021.
[33] M. A. Lejeune, "Pattern-based modeling and solution of probabilistically constrained optimization problems," *Oper. Res.*, vol. 60, no. 6, pp. 1356–1372, 2012.
[34] M. A. Lejeune and F. Margot, "Solving chance-constrained optimization problems with stochastic quadratic inequalities," *Oper. Res.*, vol. 64, no. 4, pp. 939–957, 2016.
[35] M. Alhazmi, P. Dehghanian, M. Nazemi, and K. Oikonomou, "Uncertainty-informed operation coordination in a water-energy nexus," Electronic Appendix, Accessed: Aug. 5, 2022. [Online]. Available: https://drive.google.com/file/d/1HjHyTYN_2nez-CuXPsN5VWBgnrEYCvz6/view?usp=sharing
[36] R. Fourer, D. M. Gay, and B. W. Kernighan, "AMPL. A modeling language for mathematical programming," 1993.

Mohannad Alhazmi (Member, IEEE) received the B.Sc. degree from Umm Al-Qura University, Mecca, Saudi Arabia, in 2013, and the M.Sc. and the Ph.D. degrees from The George Washington University, Washington, DC, USA, in 2017 and 2022, respectively, all in electrical engineering.

He is an Assistant Professor with the Department of Electrical Engineering, King Saud University, Riyadh, Saudi Arabia. His research interests include power system reliability and resiliency, as well as the operation of interdependent critical infrastructures.

Dr. Alhazmi was a recipient of the 2022 IEEE Industry Application Society (IAS) Electrical Safety Prevention through Design Student Education Initiative Award.

Payman Dehghanian (Senior Member, IEEE) received the B.Sc. degree from the University of Tehran, Tehran, Iran, the M.Sc. degree from the Sharif University of Technology, Tehran, Iran, and the Ph.D. degree from Texas A&M University, College Station, TX, USA, in 2009, 2011, and 2017, respectively, all in electrical engineering.

He is an Assistant Professor with the Department of Electrical and Computer Engineering, The George Washington University, Washington, DC, USA. His research interests include power system reliability and resilience assessment, data-informed decision-making for maintenance and asset management in electrical systems, and smart electricity grid applications.

Dr. Dehghanian was the recipient of the 2014 and 2015 IEEE Region 5 Outstanding Professional Achievement Awards, the 2015 IEEE-HKN Outstanding Young Professional Award, the 2021 Early Career Award from the Washington Academy of Sciences, and the 2022 Early Career Researcher Award from the George Washington University.

Mostafa Nazemi (Member, IEEE) received the B.Sc. degree in electrical engineering from the K. N. Toosi University of Technology, Tehran, Iran, the M.Sc. degree in energy systems engineering from the Sharif University of Technology, Tehran, Iran, and the Ph.D. degree in electrical engineering from The George Washington University, Washington, DC, USA, in 2015, 2017, and 2022, respectively.

He is an Electrical Engineer with MPR Associates, Inc. His research interests include power system resilience, power system planning and operation, energy optimization, and smart electricity grid applications.

Dr. Nazemi was the recipient of the 2018 Certificate of Excellence in Reviewing by the Editorial Board Committee of the Journal of Modern Power and Clean Energy for his contributions to the journal.

Konstantinos Oikonomou (Member, IEEE) received the B.Sc. degree in physics from the University of Patras, Patras, Greece, the first M.Sc. degree in energy engineering from the University of Durham, Durham, U.K., the second M.Sc. degree in electrical engineering from The George Washington University, Washington, DC, USA, and the Ph.D. degree in electrical engineering from the University of Utah, Salt Lake City, Utah, USA, in 2009, 2011, 2015, and 2019.

He is an Electrical Engineer with the Energy and Environment Directorate, Pacific Northwest National Laboratory, Richland, Washington, DC, USA, where he studies the operation, optimization, economics, and resilience of interdependent critical infrastructures.